DAKO, Glostrup, Denmark) at 20°C for 10 min. This was followed by reaction with the following primary antibodies, respectively, at 4°C overnight: monoclonal anti-proliferating cell nuclear antigen (PCNA) antiserum (mouse, PC10, NC-012, Lot. 499, Novocastra Laboratory, Newcastle, United Kingdom); polyclonal anti-S-100 protein (rabbit, Lot. 089Ec, DAKO); monoclonal anti-chondroitin-4-sulfate proteoglycan (mouse, Di-4S, Lot. 93901, Seikagaku Kogyo, Tokyo). The sections were further reacted with LINK (biotinylated anti-mouse and anti-rabbit immunoglobulins in PBS, containing carrier protein and 15 mM sodium azide, LSAB kit, DAKO) at 20°C for 60 min, and allowed to react with streptavidin solution (streptavidin conjugated to horseradish peroxidase in Tris–HCl buffer, LSAB kit, DAKO) at 20°C for 30 min. To visualize the peroxidase color reaction, the sections were incubated with DAB solution (DAB, CB090, Dojin Chemicals, Kumamoto, Japan) at 20°C for 10 min. Nuclear counterstaining was carried out with hematoxylin). Sections stained for chondroitin 4-sulfate proteoglycan were pretreated with chondroitinase ABC (Lot. KE94801 Seikagaku Kogyo), and then reacted with avidin-FITC (Lot. 090617, E.Y. Laboratory, San Mateo, CA) after reacting with the streptavidin solution. The FITC fluorescence was observed under a confocal laser scanning microscope (CLSM, LSM-GB, Olympus, Tokyo). Argon laser was used as the light source with 488 nm as the excitation light The FITC image was superimposed on the differential interference image on the background histology.

Alkaline phosphatase staining

Tissues were prepared for ALP staining according to the method described by Watanabe and Fishman [30]. The entire vertebral column was dissected en bloc and bisected sagittally in the median plane followed by fixation in 10% buffered formaldehyde for 24 h at 4°C, and further decalcified for 4–7 days in 0.5 M EDTA at 4°C. The 10 μm frozen sections were allowed to thaw in a reaction solution containing 10 mg naphthol AS-BI phosphate acid sodium salt (Lot. CAN9061, Wako Chemicals) and 10 mg Fast red violet LB salt (Lot. 07911PT, Andrich, UK) dissolved in 20 ml 0.05 M Tris–HCl buffer. After washing with water, nuclear counterstaining was carried out with hematoxylin, and mounted with glycerin (Lot. SDQ1161, Wako Chemicals).

Results

H&E stained sections with casting of microvascular meshes

In 22-week-old *twy/twy* mouse, there were osseous lesions in the longitudinal ligament between both upper and lower vertebral columns, compared to control mouse (Fig. 1). At the age of 6 weeks, the volume of the nucleus pulposus in the intervertebral discs of all regions of *twy/twy* mice began to increase causing herniation into the anterior and posterior regions, although the nucleus moved mainly in the latter direction. Herniation of the nucleus pulposus subsequently caused irregular rupture of the annulus fibrosus cartilaginous tissue. The ruptured annulus fibrosus cartilaginous cells showed reactive hyperplasia, and the fine meshes of new capillaries were elongated from the enthesis portions toward the tops of the protruded annulus fibrosus cartilaginous tissues (Fig. 2a). Further enlargement of the nucleus pulposus was noted with time; at the age of 18 weeks, twy mice showed a cluster of primitive mesenchymal cells resembling osteoblasts in the vicinity of newly formed vascular meshes in the longitudinal ligaments, both anteriorly and posteriorly and the fronts of the protrusions of reactively hyperplastic annulus fibrosus invaded the longitudinal ligaments, accompanied by a more abundant capillary network (Fig. 2b). At 22 weeks of age, the enlarged nucleus pulposus with herniation, and the rupture of the annulus fibrosus became extremely prominent, with marked increase in the number of osteoblast-like primitive mesenchymal cells. The herniated nucleus pulposus merged with the proper nucleus pulposus located in the center of the intervertebral disc. At this stage, enchondral ossifications began to develop in the cartilaginous cells at the fronts of the protruded and ruptured annulus fibrosus. Furthermore, ossification also occurred near the clusters of osteoblast-like cells at this stage, and both ossifications, enchondral and membranous, fused together forming osseous bridges in the longitudinal ligament between the upper and lower vertebrae (Fig. 2c).

Immunohistochemical staining

PCNA-positive cells began to appear in 6-week-old *twy/twy* mice, and continued to be observed there among the annulus fibrosus cartilaginous cells surrounding the herniated nucleus pulposus and those at the fronts of protrusions and invasions into the longitudinal ligaments (Fig. 3a). In *twy/twy* mice older than 18 weeks, when the fronts of ruptured annulus fibrosus invaded the longitudinal ligaments, large numbers of PCNA-positive cartilaginous cells were detected in the longitudinal ligaments (Fig. 3b). The calcium binding protein, S-100, was strongly and specifically positive in the annulus fibrosus cartilaginous cells and in the hypertrophic cartilaginous cells in the endplate at all ages. The cartilaginous cells invading the longitudinal ligaments protruding from the ruptured annulus fibrosus cartilaginous tissue in twy mice were also all positive for S-100 protein and increased with *twy/twy* mouse aging (Fig. 3c, d). The chondroitin 4-sulfate proteoglycan was

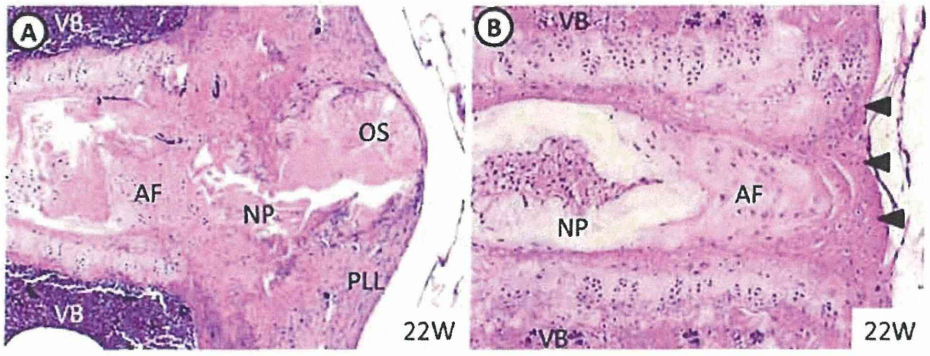

Fig. 1 Photographs showing hematoxylin and eosin (H&E) staining of 22-week-old *twy/twy* mouse cervical spine samples (**a**) and ICR mouse as a control (**b**). Compared with a control mouse, there are osseous lesions in the longitudinal ligament between both upper and lower vertebral columns in *twy/twy* mouse. *VB* vertebral body, *AF* annulus fibrosus, *NP* nucleus pulposus, *OS* osseous bridge, *PLL* posterior longitudinal ligament (*arrow heads*); magnification ×40

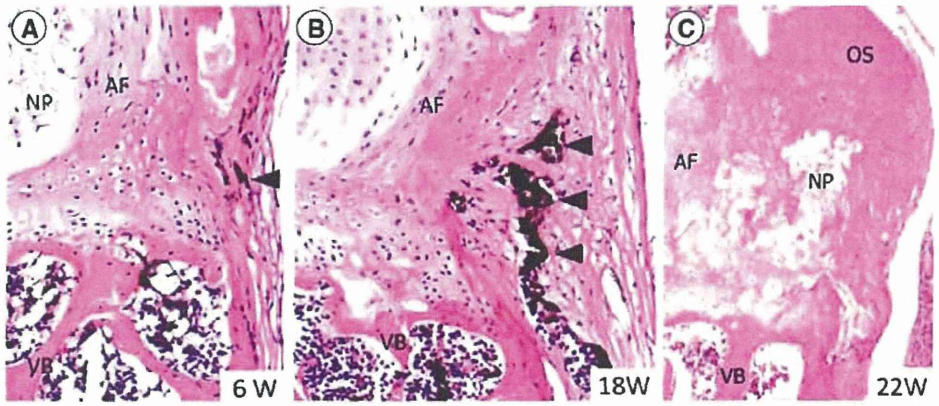

Fig. 2 Photographs showing hematoxylin and eosin (H&E) staining with casting of vascular meshes. In 6-week-old *twy/twy* mouse, the ruptured annulus fibrosus with newly produced fine meshes of capillaries (*arrowhead*) from the enthesis (**a**). In 18-week-old *twy/twy* mouse, hyperplastic annulus fibrosus invades the longitudinal ligament, together with abundant capillary meshes (*arrow heads*) (**b**). In 22-week-old *twy/twy* mouse, enlargement of nucleus pulposus with herniation and rupture of the annulus fibrosus cartilaginous tissue. Many osteoblast-like primitive mesenchymal cells are present. The herniated nucleus pulposus is continuous with the proper nucleus pulposus. Osseous bridges in the longitudinal ligament between both upper and lower vertebral columns (**c**). *VB* vertebral body, *AF* annulus fibrosus, *NP* nucleus pulposus, *OS* osseous bridge; magnification ×100 (**a**–**c**)

strongly positive in all layers of the cartilaginous tissue of the endplates at all ages, but only weakly positive in the annulus fibrosus cartilaginous tissue. However, the matrix of the herniated nucleus pulposus, and the protruded annulus fibrosus cartilaginous cells with the matrix, were strongly positive for chondroitin 4-sulfate proteoglycan in the *twy/twy* mice older than 18 weeks (Fig. 3e, f).

Alkaline phosphatase staining

ALP staining known to be positive for osteoblasts was strongly positive in the hypertrophic cartilaginous cells in the endplate. At 6 weeks of age, osteoblast-like primitive mesenchymal cells appeared in the amorphous cartilaginous tissue within the posterior part of intervertebral disc (Fig. 4a). At 10 weeks of age, ALP-positive osteoblast-like cells were markedly increased within the posterior longitudinal ligament and the intervertebral disc posteriorly (Fig. 4b). At 22 weeks of age, a number of ALP-positive small osteoblast-like mesenchymal cells were decreased with forming osseous bridges in the longitudinal ligament between the upper and lower vertebrae (Fig. 4c).

Discussion

The present histological study characterized the localization and expression of some factors related to the mechanism of cervical OPLL in the hereditary spinal hyperostotic mouse; *twy/twy* mice. The main findings of our study were: (1) the volume of the nucleus pulposus increased in all intervertebral discs causing anterior and posterior

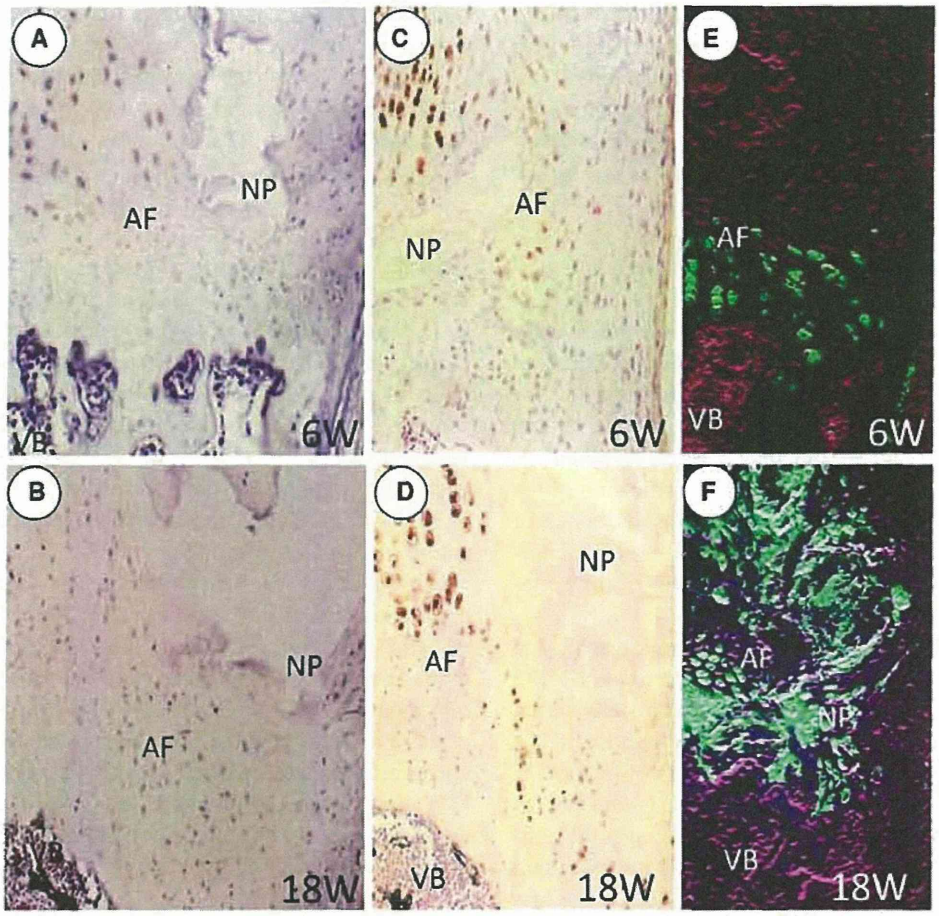

Fig. 3 Photographs showing immunohistochemical staining for proliferating cell nuclear antigen (PCNA) (**a**, **b**), S-100 protein (**c**, **d**), chondroitin 4-sulfate proteoglycan (**e**, **f**). PCNA-positive cells started to appear in 6-week-old *twy/twy* mice around the nucleus pulposus (**a**). In 18-week-old *twy/twy* mouse, the number of annulus fibrosus cartilaginous cells surrounding the herniated nucleus increased and those existing at the fronts of protrusions and invasions into the longitudinal ligament were positive for PCNA (**b**). The ruptured fibrosus cartilaginous cells and those invading the longitudinal ligament are positive for S-100 protein and increased with age (**c**, **d**). The matrix of herniated nucleus pulposus and the protruded annulus fibrosus cartilaginous cells with the matrix became strongly positive for chondroitin 4-sulfate proteoglycan with *twy/twy* mouse aging (**e**, **f**). *VB* vertebral body, *AF* annulus fibrosus, *NP* nucleus pulposus; magnification ×200 (**a**–**f**)

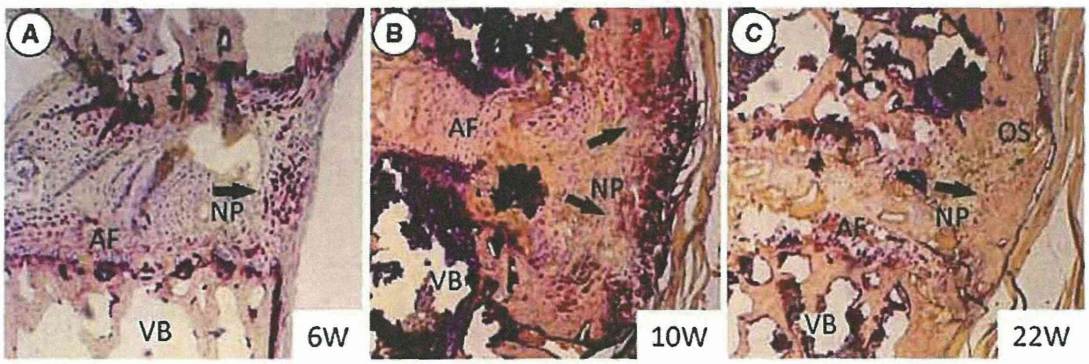

Fig. 4 Abundant ALP-positive cells (*arrows*) are found in 6-week-old *twy/twy* mouse (**a**), and the ALP-positive cells demonstrated an extensive increase in number in 10-week-old *twy/twy* mouse (**b**). In 22-week-old *twy/twy* mouse (**c**), the ALP-positive cells are decreased in number with forming osseous bridges. *VB* vertebral body, *AF* annulus fibrosus, *NP* nucleus pulposus, *OS* osseous bridge; magnification ×100 (**a**–**c**)

herniation at 6 weeks of age. The cartilaginous tissue of the annulus fibrosus was disrupted and showed regenerative proliferation with PCNA-positive cartilaginous cells. These cells were S-100 positive and the matrix was positive for chondroitin-4-sulfate proteoglycan, indicating the development of calcification; (2) over the age of 10 weeks, the regenerative cartilaginous tissue of the annulus fibrosus reached the posterior longitudinal ligament together with neovascularization and appearance of PCNA-positive proliferating primitive mesenchymal cells. These cells were considered to be osteoblasts since they were positive for ALP. Together, the serial analysis indicates that OPLL in *twy/twy* mouse is triggered by the enlargement of the nucleus pulposus followed by herniation, disruption and regenerative proliferation of annulus fibrosus cartilaginous tissues. In addition, the calcification and ossification of the longitudinal ligaments in *twy/twy* mice as a model of human OPLL seem to be primarily due to genetic abnormalities of mucopolysaccharides metabolism of the vertebral nucleus pulposus.

BMP-2 and TGF-β are thought to be involved in the development and/or progression of OPLL lesions. BMP-2 is produced in certain clusters of mesenchymal cells within the posterior longitudinal ligament at levels close to the intervertebral disc and endplate. Abnormal proliferation of chondrocytes (mostly fibrocartilage cells) is thought to contribute to the development of the early stages of ossification [11]. On the other hand, TGF-β1 plays important roles in the proliferation of fibroblast-like cells in the histologically torn posterior longitudinal ligament, fibroblasts within the non-calcified layer of the endplate cartilage and chondrocytes of the calcified zone of the endplate, thus enhancing the calcification process and ossification [11]. Within the severely degenerated posterior longitudinal ligament, a high turnover of chondrocytes and fibroblasts occurs, together with a marked proliferation of small blood vessels, particularly in the region close to the enthesis [10]. In human subjects showing hypertrophy of the posterior longitudinal ligament and OPLL, there is an associated proliferation of fibrocartilage and fibroblast-like cells within the ligament prior to ossification [24]. In this regard, the metaplastic proliferative fibrocartilage [13] may also play an important role in early ossification. Moreover, Mine and Kawai [17] have reported that undifferentiated fibroblast- and chondrocyte-like mesenchymal cells within the degenerated ligaments undergo early calcification of the supraspinous ligament, together with the proliferation of irregularly shaped fine collagen fibrils and the increased activity of acid mucopolysaccharide. In the present study, significantly large numbers of fibroblast- and osteoblast-like mesenchymal cells were noted within the posterior longitudinal ligament. These cells were also present in enthesis close to the markedly degenerated intervertebral discs posteriorly. These findings suggest that cellular proliferation contributes to the early development of OPLL.

Degeneration of the cervical intervertebral disc and vertebral endplate is thought to contribute to the progression of OPLL [15, 27]. In human subjects, histological studies have shown a high prevalence of posterior degeneration of intervertebral disc and a significant cleft formation and fragmentation, in the presence of ossified lesions [12, 27]. On the other hand, typical features of the cartilaginous endplate include a markedly irregular cleft and fissure formation as well as derangement of the calcified layer of the endplate. Although loss of ALP-positive cells is possible during histological processing of the samples, the presence of a high-ALP activity in this region, which subsequently ossifies, can be a sign of progressive enchondral ossification. The present results indicated that in the *twy/twy* mouse, development of enchondral ossification within the posterior part of the endplate occurs in close association with the membranous ossification process, which was most significant in the enthesis of the posterior longitudinal ligament. It is possible that these two ossification processes may occur simultaneously in the *twy/twy* mouse in close association with changes in matrix proteins constituting the cartilaginous endplate, such as chondroitin 4-sulfate proteoglycan or other proteoglycans [31]. Furthermore, a reconfirmation of the expression of genes related to osteogenesis, angiogenesis, and cell proliferation during an ossification process would be of great interest for future studies.

In conclusion, we showed that enlargement of the nucleus pulposus followed by herniation, disruption and regenerative proliferation of annulus fibrosus cartilaginous tissues participated in the initiation of ossification of posterior longitudinal ligament in *twy/twy* mouse. In this regard, the cells of the protruded hyperplastic annulus fibrosus invaded the longitudinal ligaments and seemed to induce neovascularization and metaplasia of primitive mesenchymal cells to osteoblasts in the spinal ligaments of *twy/twy* mice.

Acknowledgments This work was supported in part by grants (2004–2010) to HB and KU from the Investigation Committee on Ossification of the Spinal Ligaments, the Public Health Bureau of the Japanese Ministry of Labor, Health, and Welfare, and by Grant-in-Aid (B18390411, B19791023, C21591895, C21791389, B22390287, and Young Investigator grant-B22791366) to HB, HN, TY, and KU for General Scientific Research of the Japanese Ministry of Education, Science and Culture.

Conflict of interest No author has any financial ties to any commercial party related to this study.

References

1. Baba H, Furusawa N, Chen Q et al (1997) Potential role of streptozotocin in enhancing ossification of the posterior longitudinal ligament of the cervical spine in the hereditary hyperostotic mouse (*twy/twy*). Eur J Histochem 41:191–202
2. Baba H, Furusawa N, Chen Q, Imura S, Tomita K (1995) Anterior decompressive surgery for cervical ossified posterior longitudinal ligament causing myeloradiculopathy. Paraplegia 33:18–24
3. Chiba K, Yamamoto I, Hirabayashi H et al (2005) Multicenter study investigating the postoperative progression of ossification of the posterior longitudinal ligament in the cervical spine: a new computer-assisted measurement. J Neurosurg Spine 3:17–23
4. Furukawa K (2006) Current topics on pharmacological research on bone metabolism: molecular basis of ectopic bone formation induced by mechanical stress. J Pharmacol Sci 100:201–204
5. Furusawa N, Baba H, Imura S, Fukuda M (1996) Characteristics and mechanism of the ossification of posterior longitudinal ligament in the tip-toe walking Yoshimura (twy) mouse. Eur J Histochem 40:199–210
6. Furushima K, Shimoonoda K, Maeda S et al (2002) Large-scale screening for candidate genes of ossification of the posterior longitudinal ligament of the spine. J Bone Miner Res 17:128–137
7. Goto S, Yamazaki M (1997) Pathogenesis of ossification of the spinal ligaments. In: Yonenobu K, Sakou T, Ono K (eds) Ossification of the posterior longitudinal ligament. Springer, Tokyo, pp 29–37
8. Horikoshi T, Maeda K, Kawaguchi Y et al (2006) A large-scale genetic association study of ossification of the posterior longitudinal ligament of the spine. Hum Genet 119:611–616
9. Hosoda Y, Yoshimura Y, Higaki S (1981) A new breed of mouse showing multiple osteochondral lesions—twy mouse. Ryumachi 21:157–164
10. Ishida Y, Kawai S (1993) Characterization of cultured cells derived from ossification of the posterior longitudinal ligament of the spine. Bone 14:85–91
11. Kawaguchi H, Kurokawa T, Hoshino Y, Kawahara H, Ogata E, Matsumoto T (1992) Immunohistochemical demonstration of bone morphogenetic protein-2 and transforming growth factor-beta in the ossification of the posterior longitudinal ligament of the cervical spine. Spine 17:33–36
12. Kokubun S, Sakurai M, Tanaka Y (1996) Catilaginous endplate in cervical disc herniation. Spine 21:190–195
13. Lipson SJ (1998) Metaplastic proliferative fibrocartilage as an alternative concept to herniated intervertebral disc. Spine 13:1055–1060
14. Maeda S, Ishidou S, Koga H et al (2001) Functional impact of human collagen α2 (XI) gene polymorphism in pathogenesis of ossification of the posterior longitudinal ligament of the spine. J Bone Miner Res 16:948–957
15. Matsunaga S, Sakou T (2006) OPLL: disease entity, incidence, literature search, and prognosis. In: Yonenobu K, Nakamura K, Toyama Y (eds) OPLL, 2nd edn. Springer, Tokyo, pp 11–17
16. Matsunaga S, Sakou T, Taketomi E, Nakanishi K (1996) Effects of strain distribution in the intervertebral discs on the progression of ossification of the posterior longitudinal ligaments. Spine 21:184–189
17. Mine T, Kawai S (1995) Ultrastructural observations on the ossification of the supraspinous ligament. Spine 20:297–302
18. Okamoto K, Kobashi G, Washio M et al (2004) Dietary habits and risk of ossification of the posterior longitudinal ligaments of the spine (OPLL): findings from a case–control study in Japan. J Bone Miner Metab 22:612–617
19. Okawa A, Nakamura I, Goto S, Moriya H, Nakamura Y, Ikegawa S (1998) Mutation in Npps in a mouse model of the posterior longitudinal ligament of the spine. Nat Genet 19:271–273
20. Ramos-Remus C, Russell AS, Gomez-Vargas A et al (1998) Ossification of the posterior longitudinal ligament in three geographically and genetically different populations of ankylosing spondylitis and other spondyloarthropathies. Ann Rheum Dis 57:429–433
21. Resnick D, Guerra J Jr, Robinson CA, Vint VC (1978) Association of diffuse idiopathic skeletal hyperostosis (DISH) and calcification and ossification of the posterior longitudinal ligament. Am J Roentgenol 131:1049–1053
22. Resnick D, Shaul SR, Robins JM (1975) Diffuse idiopathic skeletal hyperostosis (DISH): Forestier's disease with extraspinal manifestations. Radiology 115:513–524
23. Sakou T, Taketomi E, Matsunaga S, Yamaguchi M, Sonoda S, Yashiki S (1991) Genetic study of ossification of the posterior longitudinal ligament in the cervical spine with human leucocyte antigen haplotype. Spine 16:1249–1252
24. Sato R, Uchida K, Kobayashi S et al (2007) Ossification of the posterior longitudinal ligament of the cervical spine: histopathological findings around the calcification and ossification front. J Neurosurg Spine 7:174–183
25. Seichi A, Hoshino Y, Ohnishi I, Kurokawa T (1992) The role of calcium metabolism abnormalities in the development of ossification of the posterior longitudinal ligament of the cervical spine. Spine 17:30–32
26. Shingyouchi Y, Nagahama A, Niida M (1996) Ligamentous ossification of the cervical spine in the late middle-aged Japanese men. Its relation to body mass index and glucose metabolism. Spine 21:2474–2478
27. Tanaka M, Nakahara S, Inoue H (1993) A pathologic study of discs in the elderly. Separation between the cartilaginous endplate and the vertebral body. Spine 18:1456–1462
28. Tanno M, Furukawa KI, Ueyama K, Harata S, Motomura S (2003) Uniaxial cyclic stretch induces osteogenic differentiation and synthesis on bone morphogenetic proteins of spinal ligament cells derived from patients with ossification of the posterior longitudinal ligaments. Bone 33:475–484
29. Uchida K, Nakajima H, Yayama T et al (2009) High-resolution magnetic resonance imaging and 18FDG-PET findings of the cervical spinal cord before and after decompressive surgery in patients with compressive myelopathy. Spine 34:1185–1191
30. Watanabe K, Fishman WH (1964) Application of the stereospecific inhibitor L-phenylalanine to the enzymorphology of intestinal alkaline phosphatase. J Histochem Cytochem 12:252–260
31. Yamazaki M, Goto S, Kobayashi S, Terakado A, Moriya H (1994) Bone cells from spinal hyperostosis mouse (twy/twy) maintain elevated levels of collagen production in vitro. J Bone Miner Metab 12:57–63

Mechanical compression of the spinal cord can cause neural tissue damage, reduction of neuronal cell activity and protein synthesis, and neuronal cell death by necrosis and apoptosis. Several reports have indicated that apoptosis of neurons and glial cells occurs rapidly at the level and vicinity of a traumatic insult and is followed by a secondary pathological cascade of injury in the damaged spinal cord.[1–5] Apoptotic oligodendrocytes are also found along the longitudinal axis of the spinal cord, both proximally and caudally away from the original level of injury, which contributes to delayed and prolonged demyelination and deterioration of motor function.[3,4,6,7] Because prevention of apoptosis after spinal cord injury may potentially contribute to restoration of the spinal cord neural tissue and improvement of sensorimotor function, some clinical trials have attempted to suppress apoptotic cell death after spinal cord injury with various degrees of success.[8–11]

The targeting of neurotrophic genes by retrograde transport of adenoviral vectors (AdVs) through peripheral nerves and/or targeted muscles is less invasive with the potential for repeat administration[12,13] than the direct administration of gene delivery vectors into neural tissues by intrathecal, intracerehroventricular, or intraparenchymal infusion.[14] This retrograde approach has been used for potentially therapeutic gene delivery and experimental treatments of injured central nervous system tissue, including the spinal cord.[15–17] In this context, our group has confirmed the feasibility of gene transfer of AdV-mediated brain-derived neurotrophic factor (BDNF) to spinal accessory motor neurons *via* axons innervating the sternomastoid muscle to rescue selective motor neurons damaged by acute spinal cord injury.[18,19]

On the contrary, chronic mechanical compression of the cervical spinal cord may ultimately result in an irreversible and profound motor paresis due to dysfunction, neuronal loss, and demyelination at and around the level of spinal cord compression in a fashion different from acute spinal cord injury.[20] In a series of studies,[21–25] our group examined chronic spinal cord damage using the tiptoe-walking Yoshimura (*twy/twy*) mouse,[26] a unique animal that develops spontaneous spinal cord compression at the C1–C2 vertebral level, which resembles human myelopathy. We reported previously that after the age of 18 weeks, the spinal cord in *twy/twy* mice becomes spontaneously and chronically compressed to less than 50% of its normal transverse area; this compression was associated with a progressive reduction in the number of anterior horn cells quantified through a standard labeling method and an increase in the presence of apoptotic spinal cord cells, decreased usage of neurotrophins in autocrine and paracrine interactions, axonal demyelination and the loss of axons in the white matter.[23,27,28] This *in vivo* model system thereby provides an opportunity to explore novel modes of neuroprotection against the deleterious effects of chronic mechanical compression of the spinal cord.

This study was designed to investigate the feasibility of targeted gene delivery by retrograde transport after injections of adenovirus vectors into the sternomastoid muscles of *twy/twy* mice and to examine the neuroprotective effects of the *AdV-BDNF* gene delivered in such a manner to spinal neural cells subjected to chronic mechanical compression.

MATERIALS AND METHODS

Animal Model and Intramuscular Injection of AdV

The AdV vectors carrying the BDNF (*AdV-BDNF*) or β-galactosidase (*AdV-LacZ*) genes were prepared according to the instructions provided by the supplier of the Adenovirus Expression Vector Kit (Takara Biomedicals, Ohtsu, Japan).

The Ethics Review Committee for Animal Experimentation of Fukui University approved the experimental protocol. Spinal hyperostotic *twy/twy* mice (aged 18 weeks; 22–36 g; Central Institute for Experimental Animals, Kawasaki, Japan; n = 72) were used in all experiments. Mutant *twy/twy* mice were maintained by brother-sister mating of heterozygous Institute of Cancer Research (ICR) mice (+/*twy*). The disorder is inherited in an autosomal recessive manner and the homozygous hyperostotic mouse is identified by a characteristic tiptoe walking at 6 to 8 weeks of age, but no congenital neurological abnormalities are detected at that age. The *twy/twy* mouse exhibits spontaneous calcified deposits posteriorly at the C1–C2 vertebral level, producing compression of the spinal cord between C2 and C3 cord segments. The calcified mass grows progressively with age particularly in the atlantoaxial membrane, causing profound motor paresis at the age of 20 to 24 weeks (Figure 1) with a genetal ankylosis of joints. Heterozygous ICR mice (+/*twy*) do not exhibit spontaneous calcified deposits or compression of the spinal cord; these animals (n = 4) were also used as control animals to determine whether the spinal compression that occurs in *twy/twy* mice influenced *AdV-LacZ* transfection by retrograde delivery.

The mice were anesthetized and then fixed in a supine position on a stereotaxic surgical table. The ventral aspect of the neck was sterilized followed by longitudinal incision to expose the sternomastoid muscles bilaterally, medial to the salivary glands. Using a surgical microscope, branches of the spinal accessory nerves innervating the muscles were carefully preserved. Using a microsyringe (Hamilton, Reno, NV), 25 μL of AdV-encoding *LacZ* ($\times 10^8$ PFU) (n = 38) or BDNF ($\times 10^8$ PFU) (n = 34) was injected carefully and slowly bilaterally into the middle belly of the superficial layer of each of the sternomastoid muscles simultaneously. The mouse was then allowed to recover from anesthesia and housed under a 12- to 12-hour light-dark cycle in a bacteria-free bioclean room with access to water and food *ad libitum*.

Table 1 summarizes the numbers of *twy/twy* and +/*twy* mice that were injected with *AdV-BDNF* and/or *AdV-LacZ* and how these mice were subsequently analyzed.

Tissue Harvesting and Gross Tissue Morphology

Four weeks after the intramuscular injection of *AdV-LacZ* and *AdV-BDNF* into *twy/twy* mice, or after *AdV-LacZ* injection into ICR mice, each mouse was deeply anesthetized and the cervical spinal cord was perfused and then fixed in 4% paraformaldehyde in 0.1 M phosphate-buffered saline (PBS) and postfixed in the same fixative (24 hours), 10% sucrose in 0.1 M PBS (24 hours) and 30% sucrose in 0.1 M PBS (24 hours). Segments of the spinal cord between the pyramidal decussation and C3 segment were embedded in

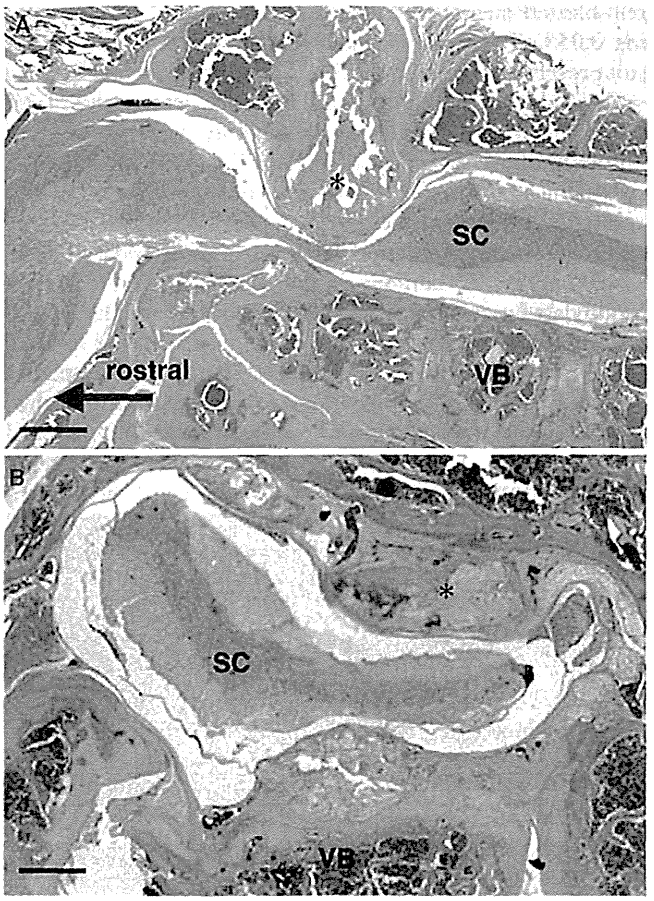

Figure 1. Photographs showing hematoxylin and eosin (H&E)-stained sagittal (A) and transaxial (B) sections of the cervical spine and the spinal cord in 22-week-old *twy/twy* mice. Calcified lesions originating from the atlantoaxial membrane in these mice grow progressively with age, compressing the spinal cord between C2 and C3 segments laterally or posteriorly. SC indicates spinal cord; VB, vertebral body. Scale bar = 500 μm. *Calcified lesions.

optimal cutting temperature compound and cut on a cryostat into serial 25-μm thick transverse frozen sections. Hematoxylin and eosin and luxol fast blue staining were performed to evaluate the gross morphology and to determine the extent of the compressed site of the spinal cord on sagittal and axial tissue sections (n = 2 sections in each orientation per group).

Immunohistochemistry

For immunofluorescence staining, the harvested tissue sections were incubated at 4°C with polyclonal rabbit antibodies against β-galactosidase (1:10,000; Abcam plc, Cambridge, UK), active caspase-3 (1:200; Abcam plc), active caspase-8 (1:100; Abcam plc), active caspase-9 (1:100; Abcam plc), $p75^{NTR}$ (1:100; Abcam plc), and 200 kD Neurofilament Heavy (NF, 1:1000; Abcam plc). Each of the aforementioned antibodies was diluted (as indicated) in Antibody Diluent with Background Reducing Components (Dako Cytomation, Carpentaria, CA). A fluorescein-conjugated goat antirabbit secondary antibody (Alexa Fluor 488, 1:250; Molecular Probes, Eugene, OR) was used to detect immunopositivity for these markers. The sections were then incubated with monoclonal mouse antibodies specific for different cell types as follows: neuronal nuclei (NeuN: 1:400; Chemicon International, Temecula, CA) as a neuronal marker; reactive immunology protein (RIP:1:100,000; Chemicon International) for mature oligodendrocytes; glial fibrillary acidic protein (GFAP: 1:400; Chemicon International) for astrocytes; microglia monoclonal antibody (OX-42, CD11b, 1:400; Abcam plc) for microglia; and NG2 (1:400; Chemicon International) for chondroitin sulfate proteoglycans present on oligodendroglial progenitor. Immunopositivity for these markers was identified using a fluorescein-conjugated goat antimouse antibody (Alexa Flour 568, 1: 250; Molecular Probes, Eugene, OR), which has emittance at a different wavelength to the secondary antibody indicated earlier. For all of the aforementioned analyses, tissue sections were harvested from a minimum of 3 animals per group.

TABLE 1. Experimental Groups Used in This Study

	AdV-LacZ–injected *twy/twy* mice	*AdV-BDNF*–injected *twy/twy* mice	*AdV-LacZ*–injected heterozygous ICR (+/*twy*) mice
Gross morphology (H&E staining)			
Axial section	2		
Sagittal section	2		
Distribution of β-galactosidase expression, LFB staining			
	4	4	4
Suppression of apoptosis			
TUNEL staining	6	6	
Immunostaining (caspase, $p75^{NTR}$)	12 (3 for each staining)	12 (3 for each staining)	
Immunoblot analysis (caspase, $p75^{NTR}$)			
	2	2	
Evaluation of NF and NG2			
Axial section	6 (3 for each staining)	6 (3 for each staining)	
Sagittal section	4 (2 for each staining)	4 (2 for each staining)	

AdV indicates adenovirus vector; BDNF, brain-derived neurotrophic factor; ICR, Institute of Cancer Research; H&E, hematoxiline & eosin; LFB, luxol fast blue; NF, neurofilament; TUNEL, terminal deoxynucleotidyl transferase–mediated dUTP-biotin nick end labeling.

The TUNEL Technique for the Detection of Apoptosis

Deoxyribonucleic acid (DNA) fragmentation was detected by terminal deoxynucleotidyl transferase (TdT)-mediated dUTP-biotin nick end labeling (TUNEL), using ApopTag Plus Fluorescein In Situ Apoptosis Detection kit (Chemicon

International). The procedures used were performed exactly as described in rhe kir manual. The reaction with TdT was terminated by washing the sections with stop-wash buffer for 2 hours at 37°C. Antidigoxigenin-Fluorescein was applied for 30 minutes at room temperature. Some sections were counterstained with nuclear marker DAPI (Abbott Molecular, Des Plaines, IL).

Microscopy

All the images were obtained *via* fluorescence microscopy (Olympus AX80; Tokyo, Japan) or confocal laser scanning microscopy (model TCS SP2; Leica Instruments, Nusslosh, Germany).

Immunoblot Analysis of the Caspase Apoptotic Pathway

Upper cervical spinal cord segments between the pyramidal decussation and C3 segment, including the maximally compressed site, were obtained from the *twy/twy* mice 4 weeks after the retrograde injection of *AdV-LacZ* (n = 2 animals) or *AdV-BDNF* (n = 2 animals) and stored in liquid nitrogen. The tissue samples were solubilized in RIPA buffer (50 mM Tris-HCl, pH 7.5, 150 mM NaCl, 1% Triton X-100, 0.5% sodium deoxycholate, 20 μg/mL leupeptine, and 1 mM phenylmethylsulfonylfluoride), homogenized, and then stored at −80°C. The protein concentration of samples was measured using the Bio-Rad DC protein assay kit (No. 500-0116; Bio-Rad Laboratories, Hercules, CA) and then equal amounts of protein (80 μg/mL) subjected to SDS-PAGE (15% gels) and Western blotting, using standard techniques. Protein-blotted membranes were washed twice in PBS containing 0.05% Tween 20, blocked in 5% skim milk for 1 hour (to prevent nonspecific binding) and subsequently probed with polyclonal antibodies specific for active caspase-3 (1:20; Abcam plc), active caspase-8 (1:10; Ahcam plc), active caspase-9 (1:10; Abcam plc), or anti-$p75^{NTR}$ (1:10; Abcam plc) overnight at 4°C. After washes in PBS/Tween 20, immunoreactivity for each of these primary antibodies was detected using enhanced chemiluminescence, with a secondary biotin-labeled antirabbit immunoglobulin G antibody and avidin-biotinylated peroxidase complex (1:200; Envision System-HRP Labeled Polymer, Dako Cytomation). The blotted membranes (PE Applied Biosystems, Foster, CA) were then stripped and reprobed for β-tubulin levels (Abcam plc) to demonstrate equal loading and protein transfer.

Quantitation of TUNEL, NF, and NG2 Immunoreactivity

To quantify the TUNEL-positive areas, NF-positive areas, and NG2-positive areas within the spinal cord, digitized images of the axial tissue sections were obtained. Six cross-sectional images were randomly selected (out of 10–15 obtained) from each of 3 segments of the spinal cord, that is, the site of maximal compression (between C2 and C3 dorsal roots), the site that was immediately rostral to tbe site of maximal compression (between C1 ventral and C2 dorsal roots), and the site that was immediately caudal to the site of maximal compression (between C3 and C4 dorsal roots). The immunopositive area in these digitized images for each fluorescence stain was then determined using grain counting, with the light intensity

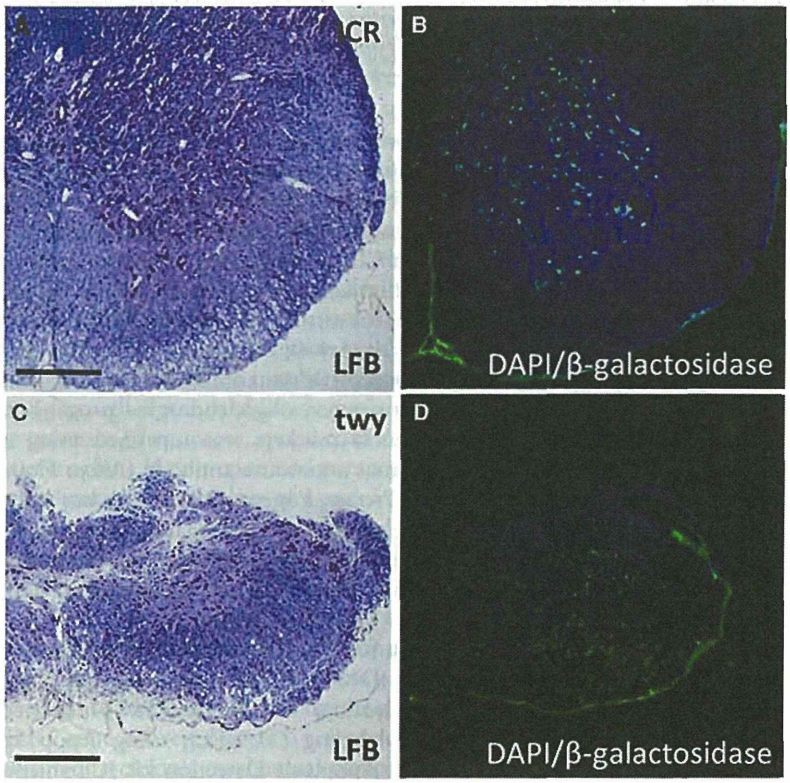

Figure 2. Photomicrographs showing LFB staining (**A** and **C**) and immunofluorescence (**B** and **D**) for β-galactosidase in the control ICR mice (**A** and **B**) and the *twy/twy* mice (**C** and **D**) 4 weeks after retrograde *AdV-LacZ* injection. DAPI/β-galactosidase-positive cells are distributed mainly in the gray matter of the spinal cord in the ICR mice (**A** and **B**), whereas in the *twy/twy* mice they are widely present in both gray and white matters at the site of maximal compression (**C** and **D**). Scale bar = 500 μm. ICR indicates Institute of Cancer Research; LFB, luxol fast blue.

set automatically by a color image analyzer (MacSCOPE; Mitani, Fukui, Japan). For TUNEL immunoreactivity, the results have been given as relative values, in which the value for TUNEL immunoreactivity in the site of maximal compression of *AdV-LacZ*–injected mice was taken as 100%. The use of these automated systems limited the potential for interpretative bias in results obtained.

Statistical Analysis

The Mann-Whitney *U* test was used to compare both the relative expression values in TUNEL staining and also differences in NF and NG2 immunostaining in each region of *AdV-LacZ* and *AdV-BDNF*–injected *twy/twy* mice. All values were expressed as means ± standard error of the mean. *P* values of less than 0.05 have denoted the presence of a significant difference between groups.

RESULTS

β-galactosidase Expression in the Compressed Spinal Cord of *twy/twy* Mice After Retrograde Gene Delivery

Immunofluorescence-stained axial tissue sections were evaluated for retrograde gene delivery in control ICR and *twy/twy* mice spinal cords injected with the *AdV-LacZ* adenoviral vector. β-galactosidase (*LacZ*)-expressing cells were observed in the gray matter in control ICR mice (Figure 2A, B), whereas they were observed in both the gray and white matters of the spinal cord of *twy/twy* mice (Figure 2C, D). To identify the distribution of transfected cells in detail, dual immunolabeling was also performed for cell-specific markers and β-galactosidase. In the *twy/twy* mice, the expression of β-galactosidase appeared not only in neurons (NeuN-positive cells), but also, in oligodendrocytes (RIP positive), astroglial

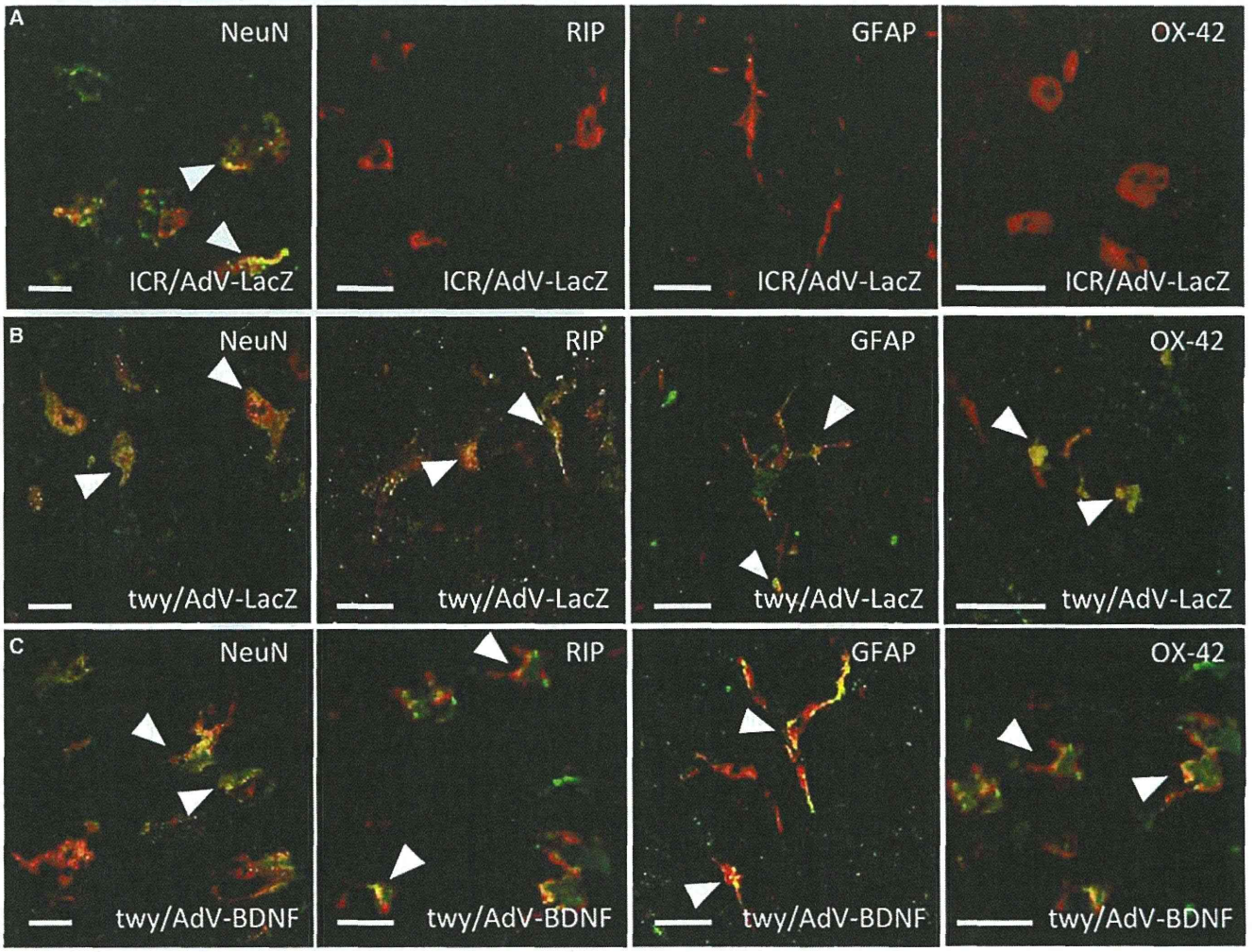

Figure 3. Photomicrographs show double-stained immunofluorescence for β-galactosidase and cell-specific markers in the spinal cord of the control ICR mice (**A**) and the *twy/twy* mice 4 weeks after retrograde *AdV-LacZ* (**B**) and *AdV-BDNF* (**C**) injections. Although expression of β-galactosidase was evident in only neurons (NeuN), including the cervical spinal motoneurons, in the control ICR mice (**A**) β-galactosidase immunoreactivity could be seen not only in NeuN but also in oligodendrocytes (reactive immunology protein [RIP]), astroglial cells (glial fibrillary acidic protein [GFAP]), and microglia (OX-42) at the site of maximal compression after retrograde gene delivery of *AdV-LacZ* (**B**) or AdV-BDNF (**C**) in the *twy/twy* mouse. White arrowheads indicate colocalization (yellow) of β-galactosidase (green) and each cell-specific marker (red). Scale bar = 10 μm. ICR indicates Institute of Cancer Research; BDNF, brain-derived neurotrophic factor.

cells (GFAP positive), and microglia (OX-42 positive) at the site of maximal compression after retrograde *AdV-LacZ* (Figure 3B) and *AdV-BDNF* (Figure 3C) gene delivery. In contrast, the expression of β-galactosidase was evident only in neurons (NeuN-positive cells), including the cervical spinal motor neurons, in the control ICR mouse (Figure 3A).

Retrograde *AdV-BDNF* Gene Delivery Protects Spinal Cord Neurons and Oligodendrocytes From Apoptotic Cell Death

Immunohistological analyses were performed to assess the effects of retrograde *AdV-BDNF* compared with *AdV-LacZ* (control) gene delivery on the apoptotic cell death pathway in cells in the compressed spinal cord of the *twy/twy* mice. The number of TUNEL-positive cells was decreased in the gray and white matters of the spinal cord after *AdV-BDNF* injection (Figure 4B) compared with *AdV-LacZ* injection (Figure 4A). Quantitative image analysis demonstrated that there was a significant proportional decrease in TUNEL immunopositivity (per cross-sectional area), at both the sites of maximal compression and also the sites rostral and dorsal to that compression, in the spinal cords of *AdV-BDNF*–injected *twy/twy* mice compared with *AdV-LacZ*–injected *twy/twy* mice (Figure 4C).

We compared the protein expression levels and distribution of active caspase-3, caspase-8, caspase-9, and $p75^{NTR}$ after retrograde *AdV-BDNF versus AdV-LacZ* gene delivery by immunoblotting of extracted proteins and immunohistology of tissue sections. Protein levels of active caspase-3, caspase-8, caspase-9, and $p75^{NTR}$ were decreased after *AdV-BDNF* injection compared with *AdV-LacZ* injection in immunoblot analysis (Figure 5A). In addition, there was decreased immunoreactivity for active caspase-3, -8, -9, and $p75^{NTR}$ in the neurons (NeuN-positive cells) and oligodendrocytes (RIP-positive cells) of *AdV-BDNF*–injected mice compared with *AdV-LacZ*–injected mice (Figure 5B–Q). This evident protection of compressed spinal neurons and oligodendrocytes from the apoptotic cell death pathway was further indicated by immunostaining for NF (neuronal) and NG-2 (oligodendrocyte precursor) as markers, where quantitative image analysis demonstrated significant increases in NF-immunoteactivity (Figure 6) and NG2-immunoreactivity (Figure 7) in the *AdV-BDNF* injected compared with *AdV-LacZ* injected *twy/twy* mice, rostral and caudal to the compression site but not in the compression site itself.

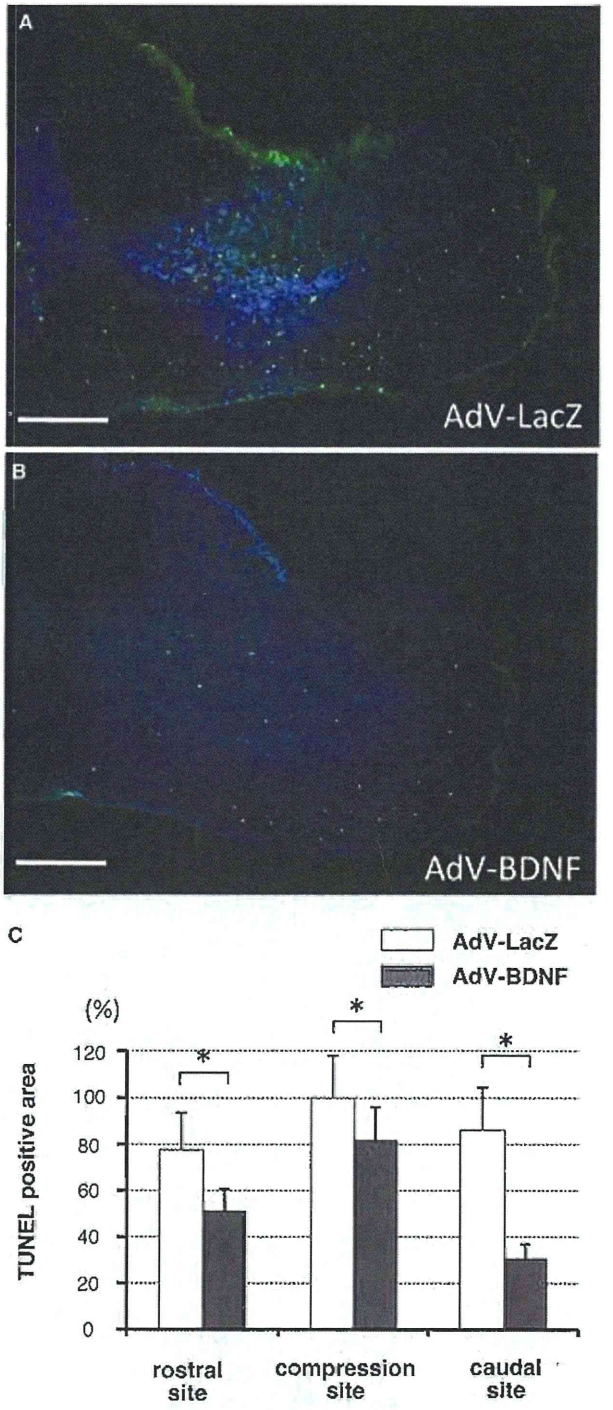

Figure 4. Photomicrographs showing TUNEL immunofluorescence staining at the site of maximal compression in the spinal cord of the *twy/twy* mice after *AdV-LacZ* gene (**A**) and *AdV-BDNF* gene (**B**) transfection. The prevalence of apoptotic (TUNEL-positive) cells in the *AdV-BDNF* gene-injected *twy/twy* mice was lower than that seen in *twy/twy* mice injected with the *AdV-LacZ* gene. The areas of TUNEL positivity (indicating the presence of apoptotic cells) at all 3 anatomic sites measured in the vicinity of the compressed spinal cord were significantly smaller in the *AdV-BDNF* gene–transfected *twy/twy* mice (n = 6) than in the *AdV-LacZ* gene–transfected *twy/twy* mice (n = 6) (**C**). Data are mean ± SD. *$P < 0.01$. Scale bar = 500 μm (**A** and **B**).

DISCUSSION

This study has used an *in vivo* model to examine the feasibility of retrograde gene delivery using adenovirus vectors into mechanically compressed cervical spinal cord tissues and, further, to determine the effects of induced BDNF gene expression delivered in such a manner. The main findings of the study are the following:

1. Retrograde gene delivery of the *LacZ* marker gene *via* the bilateral sternomastoid muscles succeeded in tranfecting the cervical spinal neurons and glial cells including oligodendrocytes in *twy/twy* mice.